

Plasma evolution induced by spatiotemporally focused femtosecond laser pulses

Wei Chu^{a,*}, Zhaohui Wang^a, Bin Zeng^a, Guihua Li^a, Fei He^a, Ya Cheng^a

^aShanghai institute of optics and fine mechanics, Shanghai 201800, China

Abstract

We report on experimental observations of formation and evolution of transient plasma produced in fused silica glass with spatiotemporally focused (STF) femtosecond laser pulses using a pump-probe shadow imaging technique. The track of the plasma is significantly curved with the STF scheme, which is attributed to an asymmetric density distribution of the transient plasma produced in the focal volume caused by the pulse front tilt of the STF laser field. In addition, strong second harmonic generation (SHG) in argon(Ar) gas induced by use of spatio-temporally focused (SF) femtosecond laser pulses was demonstrated.

© 2016 The Authors. Published by Bayerisches Laserzentrum GmbH

Keywords: spatiotemporally focusing

1. Introduction

In recent years, femtosecond laser pulses interact with transparent materials has attracted significant attention and promises a wide range of intriguing applications in many research fields. On one hand, when the femtosecond laser pulses are tightly focused in transparent materials, nonlinear interactions such as multiphoton absorption and avalanche ionization are efficiently confined within the focal volume, leading to the generation of a dense electron plasma. Such a transient plasma may induce a permanent micro- or nanoscale internal modification of bulk transparent materials, which provides the unique capability of 3-D microand nanofabrication. On the other hand, when an intense femtosecond laser pulse is focused into gases, tunnel ionization can be induce as one of the most fundamental processes for molecules in intense laser fields. Although significant effort has been made for understanding the underlying mechanisms behind the above-mentioned phenomena, the complete physical pictures are still lacking. Nevertheless, despite the incomplete understandings on these discoveries, some of the effects have already found important applications in integrated optics and microfluidics. Moreover, for high precision 3D micro and nanomachining, control of these novel phenomena at micrometer and even nanometer scales requires precise tailoring of light field within a focal spot, including the spatial (in all three dimensions) and/or temporal profiles, polarization direction, pulse front tilting, etc [1–4]. In particular, the simultaneous spatial and temporal beam shaping technique (also named “simultaneous spatial and temporal focusing (SSTF)”, “space-time focusing” or “temporal focusing (TF)”), which was originally developed for bio-imaging applications [5, 6], has been recently used in femtosecond laser micromachining of transparent materials, aiming at improving axial fabrication resolution [7, 8], eliminating nonlinear self-focusing [9, 10], and increasing the fabrication efficiency [11].

Interestingly, it was discovered that the spatiotemporally focused spot has some unconventional characteristics, in addition to the varying pulse width during propagation, including a tilted pulse front [10] and a tilted peak intensity distribution [12]. In particular, the tilted pulse front can induce a nonreciprocal writing effect which gives rise to an anisotropic fabrication quality depending on the direction of sample translation inside an isotropic medium. Until now, the mechanism behind the nonreciprocal writing effect has not been fully understood, although the intimate connection of this effect to the plasma dynamics controlled by the pulse front

* Corresponding author. Tel.: +86-21-69918441; fax: +86-21-69918021 .
E-mail address: chuwei0818@qq.com

tilt (PFT) of femtosecond pulses has been confirmed by several recent investigations [10,13]. Here, to look into the insight of the nonlinear interaction of spatiotemporally focused pulses with transparent materials, we employ a pump-probe shadow imaging technique to observe the formation and evolution of the transient plasma induced by the STF pulses [14,15]. In addition, we find that, with the SF femtosecond laser beam, it is possible to control the plasma dynamics on a femtosecond time scale, which leads to more efficient SHG in Ar as compared with conventional focusing (CF) excitation schemes using a transform-limited Gaussian beam.

2. Plasma evolution in glass induced by spatiotemporally focused femtosecond laser pulses

2.1. Experimental setup

Figure 1 schematically illustrates the experimental setup. The femtosecond laser system (Legend-Elite, Coherent, Inc.) consists of a Ti:sapphire laser oscillator and amplifier, and a grating-based stretcher and compressor that delivers 4 mJ, 50 fs pulses with a spectral bandwidth of ~ 26 nm centered at 800 nm wavelength at 1 kHz repetition rate. During the experiment, the femtosecond laser system operated in the single shot mode. Before the amplified laser beam was recompressed, it was split into two beams using a 1:1 beam splitter. One beam, which was used to produce the spatiotemporally focused pump beam, was spatially dispersed along the x direction by a pair of 1500 lines/mm gratings (blazing at $\sim 53^\circ$). More details on the arrangement of the gratings can be found elsewhere [12]. A half-wave plate and a variable neutral density filter were inserted in series before the gratings to adjust the power and the polarization of the pump beam. After being dispersed by the grating pair, the beam size was reduced to ~ 10 mm ($1/e^2$) along the x -axis and 2 mm ($1/e^2$) along the y -axis using a telescope system consisting of a convex lens ($f = 50$ cm) and a concave lens ($f = -10$ cm). We took great care in achieving the best alignment to ensure the generation of the shortest (i.e., dispersion free) pulse and the smallest focal spot at the focal plane by maximizing the brightness of the air plasma induced by the spatiotemporally focused pulses. The beam was then focused into a fused silica glass sample at a depth of ~ 250 μm below the surface using an objective lens ($20\times$, NA = 0.40). The glass samples have a size of 5 mm \times 5 mm \times 1 mm, and are polished on all the six sides. The other beam was compressed to 50 fs pulses by passing through the compressor to generate the probe beam. A pump-probe delay line was inserted into the optical path of the probe beam to adjust the relative time delay between the two beams. The interaction region in the sample was illuminated by the probe beam and then imaged with an objective lens ($10\times$, NA = 0.30) on a CCD camera. Note that the propagation direction of the probe beam was always perpendicular to the plane of the spatial chirp of the pump beam as shown in Fig. 1. A bandpass filter centered at 800 nm (40 nm bandwidth) was inserted in front of the CCD camera to filter out the emission from the laser induced plasma. For the single-shot measurement required by our investigation, the sample was shifted to a fresh area after each shot of the laser pulse. Since we are more interested in observation of spatial property of the plasma generated inside glass rather than the plasma dynamics, we define the zero time delay ($\Delta t = 0$ fs) as the moment the transient plasma appeared in the field of view (i.e., for the zero time delay defined here, the pump and probe pulses do not necessarily overlap in time).

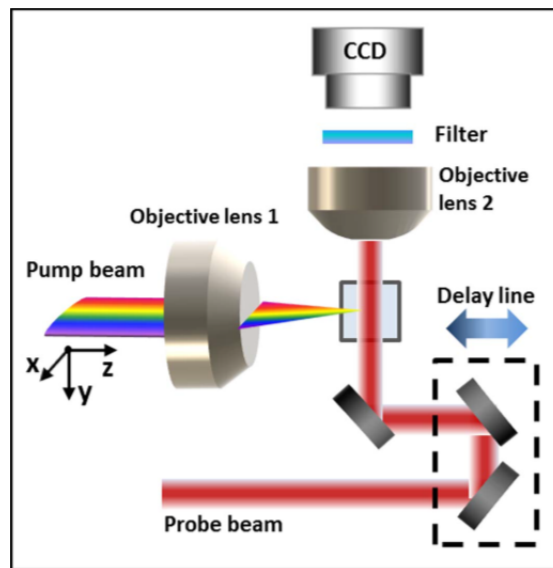


Fig. 1. Schematic of the experimental setup.

2.2. Result and discussion

Figure 2 shows a series of shadowgraphs of the transient plasma induced by the spatiotemporally focused pulse recorded at different time delays. The polarization direction of the pump laser pulse was set along x axis (see, Fig. 1) which was parallel to the spatial chirp. The pump pulse was incident from the left, and the pulse energy was set to be 6 μJ . The direction of the pulse front tilt, which indicates the sweeping direction of the pulse front in the focal volume, is from the top side to the bottom as indicated in Fig. 2. By using the theoretical analysis in the previous work [12,18], the value of the PFT (i.e., the degree of the temporal shift of the pulse peak along the x axis) in the focal plane is calculated to be 50 fs/ μm based on our experimental parameters. It should be noted that such a large PFT usually does not exist in conventional femtosecond laser pulses even if the laser system is not perfectly aligned. The dark region in these shadowgraphs results from the absorption of the probe beam by the laser-induced electron plasma inside the glass. When the time delay is short ($\Delta t < 200$ fs), the absorption of the probe beam increases with the increasing time delay. At the time delay of $\Delta t = 200$ fs, the absorption was maximized, which indicates that the density of the plasma reached the peak. At the longer time delays, the plasma started to decay due to the recombination of the electrons. Remarkably, it can be observed that the track of the plasma was bent during its propagation. A bending angle of $\sim 8^\circ$ was formed between the track of the plasma and the optical axis of the lens.

For comparison, we performed the same set of experiments using a CF system, which was achieved by simply replacing the grating pair with a pair of flat gold mirrors. Since the CF system produces a longer plasma track due to the low numerical aperture and the removal of the temporal focusing effect, the pulse energy was decreased to 2.5 μJ to avoid the ionization on the surface of the sample. As shown in Fig. 3, at the smallest time delay of $\Delta t = 0$ fs, a weak plasma was formed by the laser induced photoionization. With the increasing time delay, the plasma channel extends its length along the propagation direction of the pump pulse, which can be understood as a combined effect of the propagation of the laser pulses in the self-focused region and the survival of the laser produced plasma within its limited lifetime. At a time delay of $\Delta t = 300$ fs, the plasma channel formed in the early stage during the propagation of the pump pulses (e.g., the plasma appeared closer to the front surface as shown in Fig. 3(a)) started to decay. Meanwhile, the plasma channel kept extending its length along the propagation direction, resulting in a total plasma length of ~ 180 μm as shown in Fig. 3(h), which is much longer compared with the plasma lengths obtained by the STF system in Fig. 2. Moreover, unlike the results obtained with the STF system, the plasma tracks appear perfectly straight in Fig. 4 due to the symmetrical geometry of the Gaussian-like focal spot produced in the glass sample by the CF system.

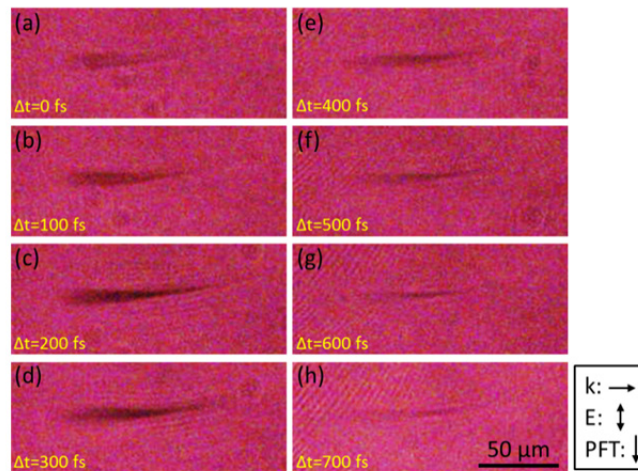


Fig. 2. Time-resolved shadowgraphs of transient plasma induced by the STF femtosecond pulse inside fused silica glass when the polarization direction of the pump pulse is parallel to the spatial chirp. The time-delay is directly indicated in each panel. The directions of the laser propagation, polarization of the laser pulse, and the PFT are indicated by the arrows next to the image.

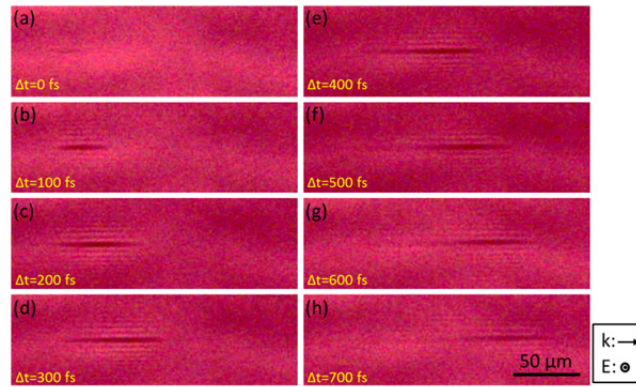


Fig. 3. Time-resolved shadowgraphs of transient plasma induced by the CF femtosecond pulse inside fused silica glass. The time-delay is directly indicated in each panel. The propagation and the polarization directions of the pump laser pulse are indicated by the black arrows next to the image.

Based on the strong dependence of the bending angle on the peak intensity and the polarization direction of the femtosecond laser pulses, we tentatively attribute the bending of the plasma track to an asymmetric plasma expansion during the interaction of the STF pulses with the fused silica glass. Here, the PFT in the focal plane of the STF spot reaches $50 \text{ fs}/\mu\text{m}$, i.e., the intensity front of the pulse rapidly sweeps across the focal plane at a velocity of $2 \times 10^7 \text{ m/s}$, which is only about one order of magnitude smaller than the phase velocity of light in fused silica. Therefore, in the cross section of the self-focused femtosecond laser beam (i.e., along the transverse plane perpendicular to the optical axis of the focal lens) produced by the STF system, the photoionization always starts from one side and sweeps across the cross section along the direction of the PFT. The rapidly moving ionization front would force the plasma to expand asymmetrically, i.e., the plasma expansion is more pronounced along a direction of the PFT than along the opposite direction. The asymmetric expansion further leads to the formation of an inhomogeneous distribution of the plasma density in the cross section of the plasma tracks.

The asymmetrical plasma density distribution will give rise to an inhomogeneous distribution of the refractive index in the focal volume. In this case, the refractive index would decrease more in the region of high-density plasma. This effect is equivalent to bending the light with a prism, as the STF pulse produces a transient wedge of plasma. Previously, it has shown that the plasma density produced by the irradiation of the femtosecond laser pulses in fused silica can be on the order of $10^{19}/\text{cm}^3$, corresponding to a refractive index change as high as 0.01 [16]. The gradient of the refractive index induced by such high-density plasma is sufficient to bend the propagation trajectory of the femtosecond pulses. Specifically, we notice that the bending direction of the plasma tracks is consistent with this scenario, because the light travelling through the plasma wedge will bend toward the region of lower plasma density (i.e., the region of higher refractive index). Furthermore, when the photoionization is stronger with the higher pulse energies used, a larger gradient of the refractive index will be created because of the enhanced asymmetry in the plasma density distribution. In this case, larger bending angles should be observed. When the CF scheme is chosen, the distribution of the plasma density always has an angular symmetry due to the Gaussian-like spatial profile of the femtosecond laser pulses. Thus only the plasma defocusing occurs which is well known in the nonlinear propagation regime. The propagation direction of the laser beam will always be along the optical axis of the focal lens, forming the straight plasma tracks as shown in Fig. 3.

3. SHG in centrosymmetric gas with spatiotemporally focused intense femtosecond laser pulses

3.1. Experimental setup

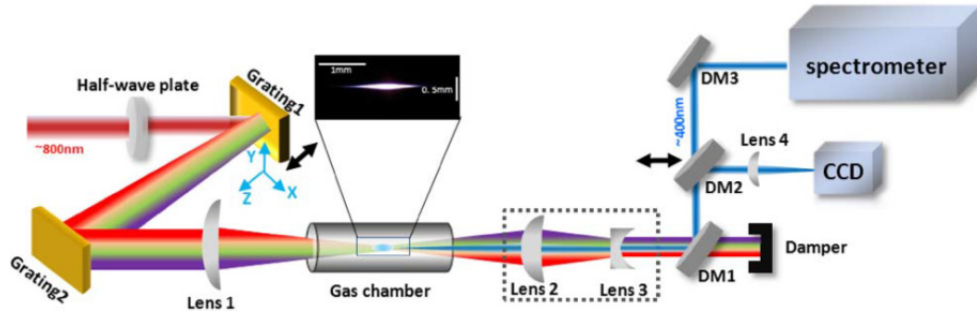


Fig. 4. Schematic of the experimental setup for generating the SHG in centrosymmetric gas.

As illustrated in Fig. 4, the experiment for generating SHG in centrosymmetric gas was carried out with a commercial Ti:sapphire laser system (Legend Elite Duo, Coherent, Inc.), which delivers ~ 6 -mJ pulses with a center wavelength at ~ 800 nm and a spectral bandwidth of ~ 30 nm at a repetition rate of 1 kHz. The amplified but uncompressed laser pulses emitted from the laser system were first spatially dispersed along the horizontal direction (i.e., X axis as shown in Fig. 4) by a pair of 1500 lines/mm gratings parallel to each other (blazing at $\sim 50^\circ$). The spatiotemporally focusing can be realized by adjusting the distance of the pair of gratings. The laser pulse of ~ 1.0 mJ was then focused by a 75-cm-focal-length lens into a chamber filled with Ar gas at a pressure of 1 bar. The generated second harmonic radiation was recorded by a spectrometer (Shamrock 303i, Andor Corp.) after its beam size being approximately reduced by half with a combination of a convex lens and a concave lens [Lens 2 ($f = 25$ cm) and Lens 3 ($f = -12$ cm), respectively]. The spatial profile of the second harmonic beam in the focal plane was imaged by a convex lens (Lens 4: $f = 20$ cm) on an area CCD camera (Wincam-d-ucd23). Three dichroic mirrors (DM1, DM2, DM3) with high reflectivity at 400 nm and high transmission at 800 nm were used to separate the fundamental beam from the second harmonic radiation. A Glan-Taylor prism before the spectrometer was used to measure the polarization of SHG. For comparison, SHG experiment with a CF scheme was also carried out by removing the grating pair while keeping all the other conditions unchanged. In this case, the transform-limited incident pulse was measured to have a pulse duration of ~ 40 fs with a nearly circular beam profile of a diameter of ~ 9 mm ($1/e^2$).

3.2. Experimental results

Figure 5 shows various properties of the second harmonic beam from Ar gas by use of SF femtosecond laser pulses. In the CF focusing scheme, the SFG can hardly be distinguished from the supercontinuum. However, when the SF focusing was employed, the second harmonic beam profile becomes a Gaussian-like distribution without any splitting, as shown in Fig. 5(a).

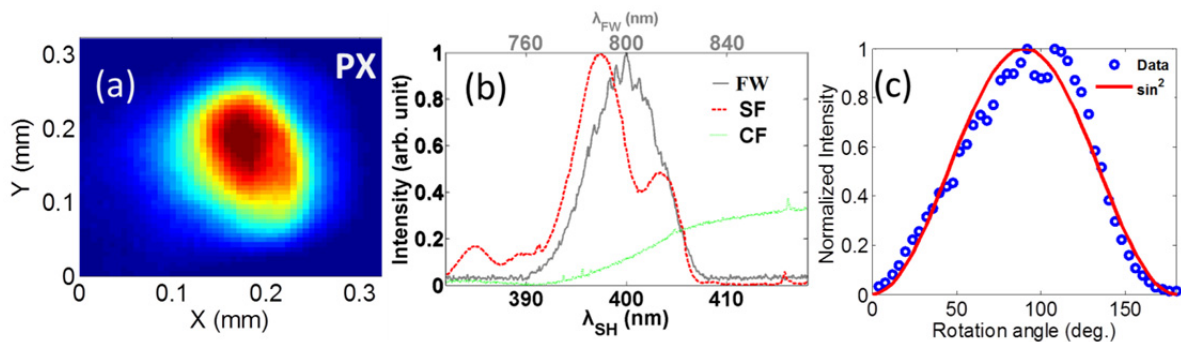


Fig. 5. The spatial patterns of SHG by the SF scheme (a); (b) The second harmonic spectra obtained in SF (red-dashed line) and the CF (green-dotted line) schemes. The fundamental wave spectrum is shown by the gray-solid curve; (c) The measured polarization property of SH for the SF case (blue circle) and the fit (red line) with $\sin^2 \theta$.

The second harmonic spectra with CF and SF schemes are also illustrated in Fig. 5(b) by the green-dot and red-dashed curves, respectively. The measured spectra are centered at ~ 400 nm, which confirms that the second harmonic of the fundamental laser pulse was indeed generated. Note that the narrow peaks appearing in Fig. 5(b)

are fluorescence emissions from Ar and very small amount of N₂ in the chamber due to the leakage. It can be seen from Fig. 5(b) that the SHG with the CF scheme (green dot line) is too weak to be distinguished from the tail of a strong supercontinuum white light, which has been generated in the filamentation process due to self-steepening and self-phase modulation. Since the white light develops progressively along the plasma filament, the much shorter filament length of ~1.5 mm produced with the SF scheme results in the dramatically reduced (almost unobservable) white light spectra as shown by the red and blue curves in Fig. 5(b). As a result, the SF laser pulses can generate second harmonic efficiently with an extremely high signal-to-noise ratio. Also we carefully checked the polarization property of the second harmonic beam obtained with the SF scheme, and found that the second harmonic is linearly polarized in the direction parallel to that of the fundamental laser, as shown in Fig. 5(c). The underlying mechanism for such remotely strong SHG by the SF scheme is ascribed to the gradient of nonuniform plasma induced by the intense SF laser field, which shows a different plasma dynamic behavior from that induced by the CF laser field.

4. Conclusion

In conclusion, we have studied the interactions between the intense STF pulses and transparent medium. The behaviors of transient plasma induced by the intense STF pulse inside fused silica glass were investigated using a pump-probe shadow imaging technique. Curved tracks of plasma distribution are observed which is unique with the STF scheme. The phenomenon can be interpreted based on the inhomogeneous plasma distributions produced in the intense STF laser field. Also we experimentally demonstrated the SHG in centrosymmetric Ar gas by use of SF linear-polarized femtosecond laser pulses. The results provides a promising way for controlling plasma dynamics in a light focal spot at the femtosecond time scale, which may find more useful applications other than the SHG in centrosymmetric media.

Acknowledgements

This work is supported by the National Basic Research Program of China (Grant Nos. 2014CB921303), National Natural Science Foundation of China (Grant Nos. 61327902, 11134010, 61275205 and 11304330).

References

- 1 R. Stoian, M. Boyle, A. Thoss, A. Rosenfeld, G. Korn, I. V. Hertel, and E. E. B. Campbell, "Laser ablation of dielectrics with temporally shaped femtosecond pulses," *Appl. Phys. Lett.* 80(3), 353–355 (2002).
- 2 Y. Cheng, K. Sugioka, K. Midorikawa, M. Masuda, K. Toyoda, M. Kawachi, and K. Shihoyama, "Control of the cross-sectional shape of a hollow microchannel embedded in photostructurable glass by use of a femtosecond laser," *Opt. Lett.* 28(1), 55–57 (2003).
- 3 C. Mauchair, A. Mermillod-Blondin, N. Huot, E. Audouard, and R. Stoian, "Ultrafast laser writing of homogeneous longitudinal waveguides in glasses using dynamic wavefront correction," *Opt. Express* 16(8), 5481–5492 (2008).
- 4 Y. Shimotsuma, M. Sakakura, P. G. Kazansky, M. Beresna, J. Qiu, K. Miura, and K. Hirao, "Ultrafast manipulation of self-assembled form birefringence in glass," *Adv. Mater.* 22(36), 4039–4043 (2010).
- 5 G. Zhu, J. van Howe, M. E. Durst, W. Zipfel, and C. Xu, "Simultaneous spatial and temporal focusing of femtosecond pulses," *Opt. Express* 13(6), 2153–2159 (2005).
- 6 D. Oron, E. Tal, and Y. Silberberg, "Scanningless depth-resolved microscopy," *Opt. Express* 13(5), 1468–1476 (2005).
- 7 F. He, H. Xu, Y. Cheng, J. Ni, H. Xiong, Z. Xu, K. Sugioka, and K. Midorikawa, "Fabrication of microfluidic channels with a circular cross section using spatiotemporally focused femtosecond laser pulses," *Opt. Lett.* 35(7), 1106–1108 (2010).
- 8 F. He, Y. Cheng, J. Lin, J. Ni, Z. Xu, K. Sugioka, and K. Midorikawa, "Independent control of aspect ratios in the axial and lateral cross sections of a focal spot for three-dimensional femtosecond laser micromachining," *New J. Phys.* 13(8), 083014 (2011).
- 9 B. Zeng, W. Chu, H. Gao, W. Liu, G. Li, H. Zhang, J. Yao, J. Ni, S. L. Chin, Y. Cheng, and Z. Xu, "Enhancement of peak intensity in a filament core with spatiotemporally focused femtosecond laser pulses," *Phys. Rev. A* 84(6), 063819 (2011).
- 10 D. N. Vitek, D. E. Adams, A. Johnson, P. S. Tsai, S. Backus, C. G. Durfee, D. Kleinfeld, and J. A. Squier, "Temporally focused femtosecond laser pulses for low numerical aperture micromachining through optically transparent materials," *Opt. Express* 18(17), 18086–18094 (2010).
- 11 D. Kim and P. T. C. So, "High-throughput three-dimensional lithographic microfabrication," *Opt. Lett.* 35(10), 1602–1604 (2010).
- 12 F. He, B. Zeng, W. Chu, J. Ni, K. Sugioka, Y. Cheng, and C. G. Durfee, "Characterization and control of peak intensity distribution at the focus of a spatiotemporally focused femtosecond laser beam," *Opt. Express* 22, 9734 (2014).
- 13 P. G. Kazansky, W. Yang, E. Bricchi, J. Bovatsek, A. Arai, Y. Shimotsuma, K. Miura, and K. Hirao, "Quill" writing with ultrashort light pulses in transparent materials," *Appl. Phys. Lett.* 90, 151120(2007).
- 14 L. Yan, X. Wang, J. Si, S. Matsuo, T. Chen, W. Tan, F. Chen, and X. Hou, "Time-resolved single-shot imaging of femtosecond laser induced filaments using supercontinuum and optical polarigraphy," *Appl. Phys. Lett.* 100, 111107 (2012).
- 15 X. Wang, L. Yan, J. Si, S. Matsuo, H. Xu, and X. Hou, "High-frame-rate observation of single femtosecond laser pulse propagation in fused silica using an echelon and optical polarigraphy technique," *Appl. Opt.* 53, 8395 (2014).